

---

# Location-Aware Pretraining for Medical Difference Visual Question Answering

---

Denis Musinguzi<sup>1</sup> Caren Han<sup>2</sup> Prasenjit Mitra<sup>1</sup>

## Abstract

Unlike conventional single-image models, differential medical VQA frameworks process multiple images to identify differences, mirroring the comparative diagnostic workflow of radiologists. However, standard vision encoders trained on contrastive or classification objectives often fail to capture the subtle visual variations necessary for distinguishing disease progression from acquisition differences. To address this limitation, we introduce a pretraining framework that incorporates location-aware tasks, including automatic referring expressions (AREF), grounded captioning (GCAP), and conditional automatic referring expressions (CAREF). These specific tasks enable the vision encoder to learn fine-grained, spatially grounded visual representations that are often overlooked by traditional pre-training methods. We subsequently integrate this enhanced vision encoder with a language model to perform medical difference VQA. Experimental results demonstrate that our approach achieves state-of-the-art performance in detecting and reasoning about clinically relevant changes in chest X-ray images.

## 1. Introduction

For certain types of diagnoses, comparing medical images of the same patient obtained at different time stamps is essential in the workflow of radiologists. This comparison enables them to assess disease progression and response to treatment. For instance, when a patient is being treated for tuberculosis (TB), multiple chest X-ray images are taken to determine whether the pathologies in the patient’s thoracic region are changing with treatment.

<sup>1</sup>Department of Electrical and Computer Engineering, Carnegie Mellon University, Kigali, Rwanda <sup>2</sup>University of Melbourne, Melbourne, Australia. Correspondence to: Denis Musinguzi <dmusingu@andrew.cmu.edu>, Prasenjit Mitra <prasenjm@andrew.cmu.edu>.

Preprint. March 6, 2026.

Visual Question Answering (VQA) involves answering questions about an image. To perform such a task, the model has to jointly interpret both image and text inputs. Several studies (Sellergren et al., 2025; Li et al., 2023a; Zhang et al., 2024; 2025) have successfully tackled the VQA task on a single medical image. However, radiologists cannot comprehensively assess a patient’s condition by examining a single image. They need to interpret multiple images to understand what changed in the patient’s body over time and thereby obtain holistic view of the patient. The medical difference VQA task (Hu et al., 2023a) proposes a setup where a model can interpret multiple images and respond to questions about them.

Medical difference VQA is more challenging than VQA because *even for the same patient, very small changes caused by a disease may not be much different from slight changes in the orientation, scale, range, view and nonrigid deformation across images* and thus may be very difficult to detect (Hu et al., 2023a). Pathologies manifest themselves in very subtle ways in chest X-ray images. Thus, models must have a *fine-grained understanding* of pathologies in order to detect changes caused by the disease while overlooking other changes (Yao et al., 2022).

Conventional architectures for medical difference VQA typically consist of a shared image encoder, a language model and a vision adapter (Cho et al., 2024; Bannur et al., 2023; Yang et al., 2025; Chen et al., 2025). In this setup, pairs of images are processed independently by the frozen encoder. To distinguish the scan order, temporal image index embeddings are added to the visual features (Bannur et al., 2023) before the vision adapter projects them into the multi-modal embedding space.

These model architectures typically rely on vision encoders pretrained on natural images, using objectives like ImageNet classification or CLIP-style contrastive learning (Radford et al., 2021; Jia et al., 2021). While they achieve strong global semantic alignment, they often lack the *fine-grained visual grounding* (Tong et al., 2024) required for tasks like medical difference VQA, where subtle regional changes are critical. Furthermore, because standard training protocols *freeze* the vision encoder, the resulting features are sub-optimal for the medical domain.

In this work, we address these limitations by introducing a

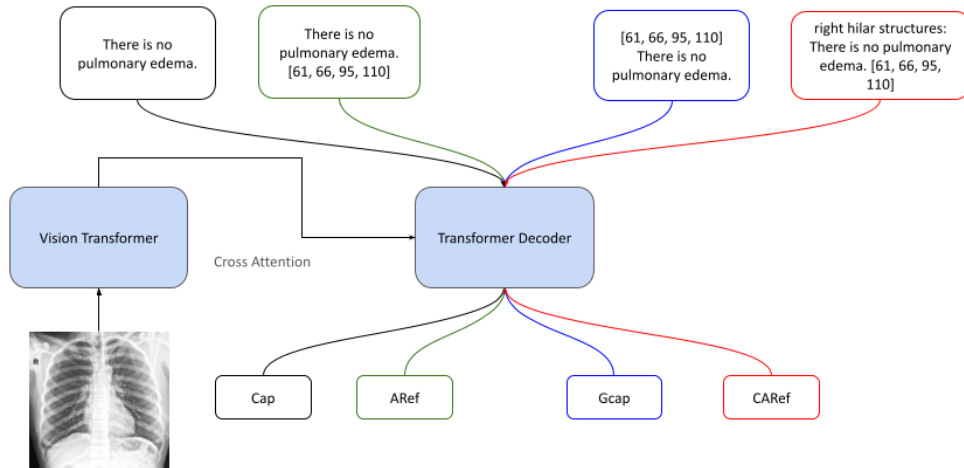


Figure 1. Overview of pretraining model architecture. The model consists of Siglip vision encoder and a transformer decoder. The vision encoder takes a chest X-ray image as input, produces visual tokens as cross attention input to the transformer decoder. We adopt the following four tasks for pretraining: Cap, AREF, GCAP and CAREF.

domain adaptive pretraining stage where the vision encoder is optimized via **location-aware objectives that enforce a fine-grained understanding of anatomical structures**. To achieve this, we adapt the multi-task generative framework (Beyer et al., 2023) by incorporating three distinct region-level supervision tasks: (i) **automatic referring expressions**, which involves predicting bounding box coordinates from automatically generated captions for specific image regions, (ii) **conditional automatic referring expressions**, which involves predicting bounding box coordinates from anatomical region names and generated captions for specific image regions and (iii) **grounded captioning**, which involves jointly predicting bounding box coordinates and captions from the image. These tasks align image regions defined by bounding boxes with their corresponding clinical descriptions, forcing the encoder to capture fine-grained visual details and spatial relationships. Subsequently, we freeze the vision encoder, and jointly finetune the multimodal projection layer and the language model for the medical difference VQA task. Our contributions can be summarized as follows:

- We propose a multimodal pretraining framework that integrates location-aware tasks—specifically grounded captioning, automatic referring expressions and conditional automatic referring expressions—into the standard auto-regressive generative training of medical vision-language models.
- We conduct comprehensive ablation studies on the proposed location-aware tasks, demonstrating that each objective contributes to representation learning, with the full synergistic combination yielding the best performance.
- We demonstrate that this grounding-centric pretrain-

ing strategy significantly enhances the vision encoder’s adaptability to the medical domain, leading to substantial improvements on the challenging medical difference VQA task.

## 2. Related Work

Advances in vision-language models (VLMs) like CLIP (Radford et al., 2021) have demonstrated impressive capabilities in global image-text alignment. However, these models primarily learn coarse, image-level semantics and struggle with the fine-grained, region-specific visual cues essential in medical imaging, where clinically meaningful findings occupy tiny regions. This limitation has motivated a shift towards pretraining strategies that explicitly model local visual semantics.

### 2.1. Vision-Language Masked Modeling

Masked modeling has emerged as a powerful alternative to contrastive learning for capturing local dependencies between images and text (He et al., 2022a; Devlin et al., 2019). By training models to reconstruct masked signals from one modality using the other, approaches like MLIP (Liu et al., 2024) eliminate the redundant background noise in global contrastive learning. However, existing multimodal methods largely rely on random masking (Kwon et al., 2022). In the medical domain, random masking poses a significant risk: it may inadvertently obscure the small, localized pathological features that define the image’s semantic content, or distort the alignment between the image and the report. Consequently, location-aware strategies are required to ensure that masking preserves, rather than destroys, the critical diagnostic regions necessary for tasks like difference VQA.

## 2.2. Local Contrastive Learning

Recent contrastive learning frameworks attempt to learn local and global representations jointly. For instance, GLoRIA (Huang et al., 2021) employs an attention-based mechanism to align image regions with individual words in the report. Yet, individual words lack sufficient semantic context to describe complex image regions, and learning this alignment without ground truth can lead to noisy associations.

Other approaches, such as VLMAE (He et al., 2022b), combine visual generative learning with contrastive learning. By recovering masked patches using regional descriptions and visible patches, the model is forced to learn local features while simultaneously using contrastive losses for global alignment. Critically, this method relies on ambiguous implicit alignment signals. In contrast, we leverage explicit region-phrase alignment provided by the chest ImaGenome dataset (Wu et al., 2021) to directly supervise the model with location-aware tasks.

## 2.3. Multi-task Generative Pretraining

Recent work (Tschannen et al., 2023; Fini et al., 2025) has demonstrated that generative captioning yields superior performance for vision–language tasks compared to contrastive learning. Building on this, the flexibility of the transformer architecture has enabled task unification via task-specific prompting (Beyer et al., 2023; Li et al., 2022; Zhang et al., 2022), allowing models to move beyond simple global descriptions to region-specific descriptions. By incorporating location-aware tasks such as grounded captioning and referring expression comprehension, models are explicitly trained to localize features (Wan et al., 2024). We leverage this property to address the high level of granularity required in medical image understanding, where precise localization of abnormalities is critical.

## 2.4. Longitudinal modeling of medical images

Approaches to medical difference VQA generally fall into three categories: feature concatenation, explicit difference modeling, and intermediate reasoning. Concatenation-based methods (Cho et al., 2024; Yao et al., 2022) process image streams via shared encoders. For instance, PLURAL (Cho et al., 2024) employs a multi-stage transfer strategy from natural images, concatenating features from prior and current scans. However, these methods typically rely on global feature alignment, often missing the fine-grained regional changes required for precise difference detection.

Difference-based methods like ReAL (Lu et al., 2024; Hu et al., 2023b) compute pixel-level residual images and pass them through a separate visual encoder. While theoretically appealing, computing residual images through subtraction is highly sensitive to spatial misalignment if no prior image

registration is performed (Lu et al., 2024), introducing noise into the VQA pipeline.

Finally, intermediate reasoning approaches such as RG-AG (Serra et al., 2025) adopt a two-stage pipeline that first generates a descriptive radiology report to serve as context for the final answer. While this leverages the reasoning power of LLMs, it creates an information bottleneck where visual nuances not captured in the intermediate text are lost. In contrast to these approaches, we propose a domain-adaptive pretraining strategy that directly enforces fine-grained, location-aware understanding without relying on fragile pixel subtraction or intermediate textual bottlenecks.

# 3. Methodology

## 3.1. Pretraining tasks

We adopt a location-aware vision pretraining strategy (Wan et al., 2024) within a multi-task generative framework (Beyer et al., 2023). Specifically, we integrate localization information into the image captioning objective (Tschannen et al., 2023) during model pretraining by utilizing task-specific prefixes and a unified decoder for multi-task training as shown in Figure 1.

Image captioning involves generating a sequence of tokens  $y = [y_1, y_2, \dots, y_n]$  describing an image input  $x$ . We prepend a prefix to the caption to specify the task. We utilize three location-aware tasks: automatic referring expressions (AREF), grounded captioning (GCAP) and conditional automatic referring expressions (CAREF). In automatic referring expressions, the model receives a description and generates the corresponding bounding box coordinates. Conversely, grounded captioning tasks the model with describing a specific image region defined by input coordinates. Finally, conditional automatic referring expressions requires the model to predict bounding box coordinates and a description based solely on an anatomical region name. The model is trained to generate both regional descriptions and bounding box coordinates sequentially based on task prefixes rather than providing either the bounding box coordinates or the regional description as inputs.

## 3.2. Model details

### 3.2.1. ARCHITECTURE

We employ a conventional encoder-decoder framework. The encoder comprises the Siglip (Zhai et al., 2023) vision encoder. A two-layer MLP with a GeLU activation is used to project the image features into the multimodal embedding space. The text is tokenized using a GPT-2 tokenizer. The tokens are converted into embeddings using a linear layer and learnable positional embeddings are added. The decoder is

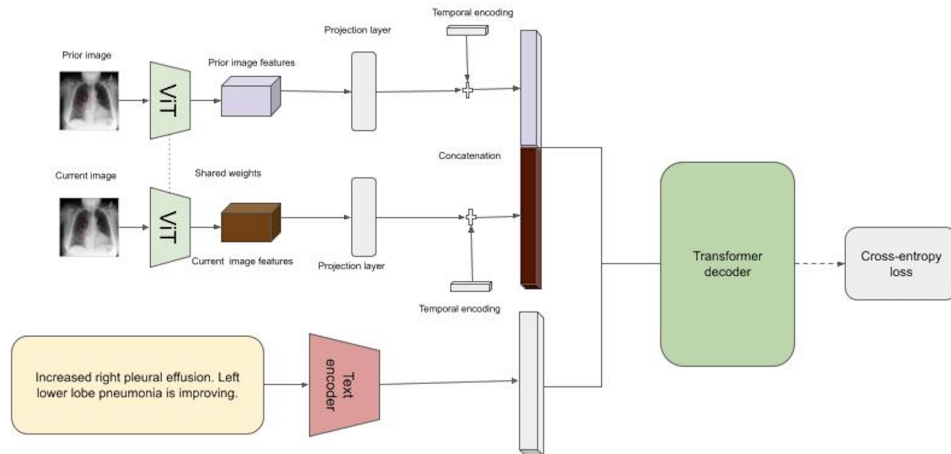


Figure 2. Overview of medical difference model architecture. The model consists of a frozen pretrained vision encoder, a vision adapter and a transformer decoder.

built on a standard transformer architecture (Vaswani et al., 2017). The decoder processes image features using cross-attention across each layer to integrate visual and textual information effectively. A causal attention mask is used to guide the prediction of each token in the sequence, making sure that each token is generated based on the ones before it at each step. Inspired by (Tschannen et al., 2023; Wan et al., 2024), we adopt parallel prediction for 25% of the training examples in the standard image captioning task. The model predicts all tokens independently and in parallel, relying solely on visual information to prevent dependence on preceding text tokens to predict subsequent ones.

### 3.2.2. OBJECTIVE

The optimization of the model parameters is achieved by maximizing the log likelihood:

$$\sum_{i=1}^{|y|} \log P_{\theta}(y_i, y_{<i}, x)$$

The model predicts captions and bounding boxes sequentially rather than predicting either the caption based on the bounding box or the bounding box based on the caption. For a fraction of the training examples, we apply parallel prediction and train the model to predict the tokens in their correct order. We achieve this by masking all the tokens and shifting the target tokens to match the expected output. We apply the loss to the entire output except the task prefix. The loss on the caption guides the model to identify a region and generate its caption, while the loss on the bounding box coordinates refines the model’s ability to accurately regress the box location relative to the caption.

## 3.3. Datasets

### 3.3.1. MIMIC-CXR DATABASE

MIMIC-CXR contains 377,110 chest X-ray images from 65,379 patients, with de-identified free-text reports describing the images (Johnson et al., 2024b; Goldberger et al., 2000; Johnson et al., 2019). The dataset has multiple studies for each patient obtained at different time stamps. Each study has multiple images taken in different views accompanied by a medical report. We followed the official train, validation and test splits. Following prior work (Sellergren et al., 2025; Yang et al., 2025), we utilized only anterior-posterior and posterior-anterior image views and findings and impression sections of the report. We removed words referring to previous studies from the chosen sections of the reports. To mitigate the storage and computational demands of large image files, we utilized JPG images from the MIMIC-CXR-JPG dataset (Johnson et al., 2024a) rather than DICOM images from MIMIC-CXR database. We utilized this dataset for the captioning task.

### 3.3.2. CHEST IMAGENOME DATASET

The Chest Imagenome dataset (Wu et al., 2021) comprises 242,072 frontal chest X-ray images derived from the MIMIC-CXR dataset. It features automatically constructed scene graphs for frontal MIMIC-CXR images. Each scene graph provides bounding boxes and corresponding phrases for the subset of the 29 anatomical regions explicitly mentioned in the radiology report. The splits in the chest Imagenome dataset follow the official splits in the MIMIC-CXR dataset.

We extracted anatomical region bounding box coordinates, region names, and corresponding descriptive phrases from the scene graphs. We created training samples for the three

location-aware tasks from each sample in the dataset. Figure 1 shows an example of each task. For AREF, the phrases were concatenated with the bounding box coordinates at the end. For GCAP, the bounding box coordinates were inserted first, followed by the combination of all phrases. For CAREF, the anatomical region name was placed first, followed by the descriptive phrases, with the bounding box coordinates at the end.

### 3.3.3. MIMIC-DIFF-VQA DATASET

MIMIC-Diff-VQA (Hu et al., 2023b) consists of 700,703 question-answer (QA) pairs derived from a subset of 164,324 longitudinal chest X-ray pairs from the MIMIC-CXR dataset. These QA pairs were generated via an automated pipeline based on original radiologist reports and are classified into seven distinct categories: difference, presence, abnormality, view, location, level, and type. For this study, we focused on the 164,324 pairs within the “difference” category, as they necessitate a comparative analysis between the reference and main images. Our experimental setup adheres to the official dataset partitioning for training, validation, and testing.

## 4. Experiments

### 4.1. Experimental setup

#### 4.1.1. IMPLEMENTATION DETAILS

We adopt an encoder-decoder model with 620 million parameters. The vision encoder is instantiated with the same architectural configuration as SigLIP (Zhai et al., 2023), featuring 27 transformer blocks, 12 attention heads, a hidden dimension of 1152, and an input patch size of 14. The decoder consists of 12 transformer blocks with 12 attention heads and a hidden dimension of 1024. We initialize the network randomly and train the entire model from scratch.

#### 4.1.2. PRETRAINING DETAILS

We pretrained the model on the image-report pairs from MIMIC-CXR database and the location-aware data extracted from the Chest Imagenome dataset for 5 epochs. Each batch contained an equal number of data samples of the four tasks. We used the AdamW optimizer ( $\beta_1 = 0.9, \beta_2 = 0.999$ ), with 5,000 linear warmup steps followed by cosine annealing schedule. The batch size is set to 32, while the learning rate and weight decay are adjusted to  $10^{-4}$  and  $10^{-2}$ , respectively. We did not apply augmentations except resizing the images to a resolution of  $448 \times 448$ . We tokenized the text using the GPT2 tokenizer (Radford et al., 2019) using a vocabulary of 50,256 tokens. We represented the bounding boxes using binned image coordinates ranging from 0 to 447. Unlike approaches that introduce specialized location tokens, we retain these integers in their

natural language format, allowing the model to generate coordinates using its existing vocabulary. We employ mixed precision with bfloat16. We train the model for 85 hours using an NVIDIA A100 GPU with 80 GB VRAM.

#### 4.1.3. VISION ENCODER EVALUATION

We evaluated the fine-grained understanding capabilities of the pretrained vision encoder on a held-out test set of grounded captioning and conditional automatic referring expressions data samples. We omitted automatic referring expressions due to inherent ambiguity, as the same expression can validly describe multiple regions, complicating ground truth comparison.

For grounded captioning, we prompted the model with a task prefix and bounding box coordinates. We evaluated the generated text using BLEU (Papineni et al., 2002), ROUGE-L (Lin, 2004), METEOR (Banerjee & Lavie, 2005), and CIDEr (Vedantam et al., 2015) (see Table 1). Conversely, for the CAREF task, we used the regional name as the prompt. We evaluated the localization accuracy using the standard Acc@0.5 metric, yielding a score of 69.8%.

Table 1. Results showing the performance of the pre-trained model on the grounded captioning task.

BLEU-4	METEOR	ROUGE-L	CIDEr
0.476	0.501	0.593	1.201

#### 4.1.4. DOWNSTREAM FINETUNING

To address the medical difference visual question answering (Medical Diff-VQA) task, we trained the model on the MIMIC-Diff-VQA dataset. The model is comprised of a pretrained vision encoder, a GPT-2 text decoder and a vision adapter (see Figure 2).

A shared vision encoder  $E_{img}$  processes both the reference image ( $i_{ref} \in \mathbb{R}^{H \times W}$ ) and the main image ( $i_{main} \in \mathbb{R}^{H \times W}$ ), where  $H = W = 448$ . Learnable temporal embeddings  $t_{enc}^{ref}, t_{enc}^{main} \in \mathbb{R}^{n \times d_v}$  are added to the respective encoder outputs to encode temporal information:

$$v_{vis}^{ref} = E_{img}(i_{ref}) + t_{enc}^{ref} \in \mathbb{R}^{n \times d_v}$$

$$v_{vis}^{main} = E_{img}(i_{main}) + t_{enc}^{main} \in \mathbb{R}^{n \times d_v}$$

$n$  represents the number of visual tokens (flattened spatial features) and  $d_v$  is the vision encoder’s output dimension. A vision adapter,  $P_{img}$  consisting of two linear layers with a GeLU activation is used to project the visual features into the multimodal embedding space.

$$v_{proj}^{ref} = P_{img}(v_{vis}^{ref}) \in \mathbb{R}^{n \times d_t}$$

Table 2. Results showing the comparative performance of various vision encoder pretraining methods, each combined with a GPT-2 decoder, on the Medical Difference VQA task. The best results are in in **bold**. Under the same training settings, our method outperforms the baselines and the state of the art approaches.

Method	BLEU-4	METEOR	ROUGE-L	CIDEr	BertScore
Location Aware Pretraining (Ours)	<b>0.594</b>	<b>0.425</b>	<b>0.747</b>	<b>2.997</b>	<b>0.972</b>
Global Contrastive Pretraining	0.291	0.300	0.407	0.550	0.850
Regional Contrastive Pretraining	0.360	0.338	0.465	0.635	0.956
BLIP-2 (Li et al., 2023b)	0.375	0.350	0.545	0.801	0.960
CapPa (Tschannen et al., 2023)	0.350	0.327	0.529	0.675	0.948
RG-AG (Serra et al., 2025)	0.551	0.384	0.668	2.198	0.965
ReAI (Lu et al., 2024)	0.530	0.395	0.736	2.409	0.968
PLURAL (Cho et al., 2024)	0.520	0.381	0.653	1.832	0.963

$$v_{proj}^{main} = P_{img}(v_{vis}^{main}) \in \mathbb{R}^{n \times d_t}$$

The question text  $t$  is tokenized using the GPT-2 Tokenizer and mapped to embeddings  $l_{txt} \in \mathbb{R}^{n \times d_t}$  via the model’s native embedding layer. The input to the decoder is constructed by prepending the visual embeddings to the text embeddings as follows:

$$Input_{seq} = [v_{proj}^{ref}; v_{proj}^{main}; l_{txt}]$$

This results in a total sequence length of  $2n + n_t$ . Positional embeddings are added to the entire concatenated sequence.

A pre-trained GPT-2 (Radford et al., 2019) medium decoder with 315 million parameters is used as the language decoder. The model is optimized using standard auto-regressive cross-entropy loss:

$$L = - \sum_{j=1}^{|y|} \log P_{\theta}(y_j | v_{proj}^{ref}, v_{proj}^{main}, l_{txt}, y_{<j})$$

where  $y$  represents the ground-truth answer tokens, and  $P_{\theta}$  represents the trainable parameters. Crucially, loss is computed on the answer tokens only.

The vision encoder is frozen, while the vision adapter and the language decoder are finetuned. The model was trained using the AdamW optimizer (learning rate =  $2 \times 10^{-4}$ , weight decay =  $1 \times 10^{-2}$ ) with a label smoothing factor of 0.11. The model was trained for 10 epochs on an NVIDIA A100 GPU (80 GB VRAM), lasting 44 hours. The learning rate followed a linear warmup schedule for 10% of the training steps, and a cosine decay schedule to zero.

#### 4.1.5. BASELINES

We evaluate our approach against seven baseline models on the difference category MIMIC-Diff-VQA dataset. To ensure a strictly controlled comparison, we implemented and trained the Global Contrastive, regional contrastive, CapPa (Tschannen et al., 2023), and BLIP-2 (Li et al., 2023b) baselines using the exact same data partitions and experimental

settings as our proposed method. Specifically, the global contrastive model employs Sigmoid loss (Zhai et al., 2023), while the regional contrastive baseline aligns image regions with regional captions to enforce fine-grained semantic correspondence. CapPa utilizes a hybrid objective combining standard autoregressive captioning with non-autoregressive parallel prediction, and BLIP-2, which bridges a frozen vision encoder and LLM via a trainable Q-Former. For the remaining baselines, we report results directly from their respective original publications. These include PLURAL (Cho et al., 2024), a generative model featuring a dedicated input branch for prior scans and a multi-stage pretraining strategy on longitudinal reports; Pixel-Difference (ReAL) (Lu et al., 2024), which explicitly inputs the computed residual image between the reference and follow-up scans; and a RG-AG (Serra et al., 2025) approach adopts a two-stage pipeline that first generates a descriptive radiology report, utilizing the text as an intermediate reasoning context to derive the final answer.

## 4.2. Quantitative Results

We compare the performance of different vision-encoder pretraining strategies, along with state-of-the-art baselines in Table 2 on the downstream task of medical difference VQA using the MIMIC-Diff-VQA dataset. We evaluated the performance using natural language generation metrics, including BLEU, METEOR, ROUGE-L, and CIDEr, which measure the similarity between generated and reference answers based on n-gram overlap and sequence alignment. Furthermore, to capture semantic equivalence beyond surface-level overlap, we utilize BERTScore (Zhang et al., 2019) with the PubMedBERT (microsoft/BiomedNLP-PubMedBERT-base-uncased-abstract-fulltext) model type.

The results demonstrate that our method outperforms the baselines across evaluation metrics, with particularly notable gains in BLEU-4 and CIDEr scores. Compared to the strongest baseline, our model achieves a relative improvement of 7.8% in BLEU-4 and a substantial 24.4% relative

Table 3. Selected test cases to qualitatively compare the outputs of our approach with those of the baselines in Medical Diff VQA. **Red** indicates incorrect or missing predictions and **green** indicates correct predictions. The examples illustrate our model’s ability to identify differences between the two images and correctly attribute them to the appropriate image. However, there are instances where the model omits certain relevant features.

Case I	Case II	Case III
Reference      Main	Reference      Main	Reference      Main
		
<b>Q:</b> What has changed compared to the reference image?	<b>Q:</b> What has changed compared to the reference image?	<b>Q:</b> What has changed compared to the reference image?
<b>GT:</b> the main image has additional findings of <b>lung opacity</b> , and <b>atelectasis</b> than the reference image.	<b>GT:</b> the main image has an additional finding of <b>atelectasis</b> than the reference image.	<b>GT:</b> the main image has additional findings of <b>cardiomegaly</b> , <b>edema</b> , <b>atelectasis</b> , and <b>pleural effusion</b> than the reference image. the main image is missing the findings of <b>lung opacity</b> , and <b>pneumonia</b> than the reference image.
<b>Ours:</b> the main image has additional findings of <b>lung opacity</b> , and <b>atelectasis</b> than the reference image.	<b>Ours:</b> the main image has an additional finding of <b>atelectasis</b> than the reference image.	<b>Ours:</b> the main image has additional findings of <b>atelectasis</b> , and <b>pleural effusion</b> than the reference image. the main image is missing the findings of <b>lung opacity</b> , and <b>pneumonia</b> than the reference image.
<b>ReAI:</b> the main image has additional findings of <b>lung opacity</b> , and <b>atelectasis</b> than the reference image.	<b>ReAI:</b> the main image has additional findings of <b>pleural effusion</b> , and <b>atelectasis</b> than the reference image.	<b>ReAI:</b> the main image has additional findings of <b>atelectasis</b> , and <b>lung opacity</b> than the reference image.

gain in CIDEr. Furthermore, we observe relative increases of 1.5% in ROUGE-L and 7.6% in METEOR score.

Our approach offers distinct advantages over state-of-the-art baselines in terms of both inference and training efficiency. First, unlike ReAI (Lu et al., 2024), we eliminate the need for computing residual images or performing image registration. Instead, we rely on the vision encoder’s learned representations to detect fine-grained abnormalities directly from the input pairs. Second, we outperform PLURAL (Cho et al., 2024) while using a significantly lighter training pipeline; whereas PLURAL requires massive multi-stage pre-training on natural and medical domains, our method achieves state-of-the-art results with a single, compute-efficient pre-training step.

### 4.3. Qualitative Results

Table 3 shows selected examples to qualitatively compare the outputs of our model and those ReAI (Lu et al., 2024).

We generate responses beam decoding with a beam size of 10. In case I, both models successfully identify the additional pathologies present in the main image. In case II, ReAI omits pleural effusion from the additional findings in the main image. Case III presents a more challenging scenario, and both models make errors. ReAI swaps lung opacity from missing to additional finding in the main image and does not generate the pathologies that are in the reference image but not in the main image. Our model also omits cardiomegaly and edema from the additional findings in the main image.

### 4.4. Ablation Study

#### 4.4.1. PRETRAINING TASKS

To assess the impact of different pretraining objectives, we conducted an ablation study focusing on the AREF, GCAP, CAREF, and captioning tasks. Specifically, we evaluated the effect of removing each task individually and removing

Table 4. Results of the ablation study when we removed some of the location aware pretraining tasks. The best results are in **bold**.

AREF	GCAP	CAREF	CAP	BLEU-4	METEOR	ROUGE-L	CIDEr
✓	✓	✓	✓	<b>0.594</b>	<b>0.425</b>	<b>0.747</b>	<b>2.997</b>
×	✓	✓	✓	0.283	0.244	0.379	0.850
✓	×	✓	✓	0.347	0.318	0.527	0.945
✓	✓	×	✓	0.347	0.316	0.533	0.946
×	×	×	✓	0.350	0.317	0.529	0.950

all the location aware tasks. All models were trained on the same dataset using the same number of examples at an image resolution of  $448 \times 448$ , and subsequently finetuned and evaluated on the medical difference VQA task. As shown in Table 4, removing all location-aware tasks leads to a substantial drop in performance across all evaluation metrics. Among the individual tasks, excluding AREF results in the largest degradation, underscoring the importance of anatomical references for strengthening region-level reasoning and supporting fine-grained visual understanding. Incorporating all location-aware tasks yields the best overall performance, demonstrating that the tasks provide complementary benefits to the encoder’s representation learning.

#### 4.4.2. PRETRAINING IMAGE RESOLUTION

Table 5 presents results for two pretraining image resolutions: 224 and 448. The models are trained under identical settings, differing only in input resolution. Each model is trained from scratch at its respective input resolution and later fine-tuned at the same resolution used during pretraining. We observe that the model trained at  $448 \times 448$  achieves consistently better performance than the model trained at  $224 \times 224$ .

Table 5. Ablation study of the impact of different image resolutions on the medical difference VQA. The best results are in **bold**.

Image resolution	BLEU-4	METEOR	ROUGE.L
$224 \times 224$	0.384	0.356	0.504
$448 \times 448$	<b>0.594</b>	<b>0.425</b>	<b>0.747</b>

#### 4.4.3. PARALLEL PREDICTION

During pretraining, we randomly mask a fraction of training examples and train the model to reconstruct the masked items in parallel while maintaining their original ordering. To understand how the masking strategy influences the quality of learned visual representations, we perform an ablation study in which we vary the masking ratio from 0 to 50%. We train the model at a resolution  $448 \times 448$  and transfer to the medical difference visual question answering task at the same resolution. As shown in Table 6 using parallel prediction for 25% of the training examples yields the

best performance. In contrast, removing parallel prediction entirely leads to a substantial decline in downstream performance of the model, and increasing its proportion to 50% similarly degrades performance. This suggests that a moderate amount of parallel prediction provides the most effective balance for learning.

Table 6. Results showing the impact of the percentage of training samples that are masked during the vision encoder pretraining on downstream performance of the vision encoder. The best results are in **bold**.

Parallel (%)	BLEU-4	METEOR	ROUGE-L
0	0.301	0.304	0.448
25	<b>0.594</b>	<b>0.425</b>	<b>0.747</b>
50	0.358	0.339	0.484

## 5. Conclusion

We introduced a location-aware pretraining strategy for vision encoders designed for the medical difference VQA task. By incorporating spatially grounded supervision, the model develops more nuanced representations of chest X-ray images and demonstrates improved sensitivity to subtle inter-image differences. Our method outperforms the previous state-of-the-art approach.

While simple, our method requires strong supervision, currently only provided by the Chest ImaGenome dataset, and can be hard to generalize to other image modalities. Additionally, despite these gains in performance, the model occasionally omits or hallucinates certain pathologies when describing differences between two images. We expect that increasing the scale and diversity of the training data would help mitigate these failure cases.

## Impact Statement

This work aims to assist radiologists by automating the detection of temporal changes in medical imaging, potentially reducing diagnostic workload and improving the identification of disease progression. However, we acknowledge the risks associated with deploying VQA models in clinical settings.

First, like many generative models, our system may be prone to hallucinations or plausible but incorrect text generation; therefore, it is intended to function strictly as a human-in-the-loop assistive tool rather than a standalone diagnostic agent. Second, while our method improves robustness to acquisition differences, the model’s performance is contingent on the diversity of the training data. Biases present in public chest X-ray datasets may propagate to the model’s predictions. Future deployment requires rigorous validation across diverse patient populations to ensure equity and clinical safety.

## References

- Banerjee, S. and Lavie, A. Meteor: An automatic metric for mt evaluation with improved correlation with human judgments. In *Proceedings of the acl workshop on intrinsic and extrinsic evaluation measures for machine translation and/or summarization*, pp. 65–72, 2005.
- Bannur, S., Hyland, S., Liu, Q., Perez-Garcia, F., Ilse, M., Castro, D. C., Boecking, B., Sharma, H., Bouzid, K., Thieme, A., et al. Learning to exploit temporal structure for biomedical vision-language processing. In *Proceedings of the IEEE/CVF Conference on Computer Vision and Pattern Recognition*, pp. 15016–15027, 2023.
- Beyer, L., Wan, B., Madan, G., Pavetic, F., Steiner, A., Kolesnikov, A., Pinto, A. S., Bugliarelli, E., Wang, X., Yu, Q., et al. A study of autoregressive decoders for multi-tasking in computer vision. *arXiv preprint arXiv:2303.17376*, 2023.
- Chen, Y., Xu, S., Sellergren, A., Matias, Y., Hassidim, A., Shetty, S., Golden, D., Yuille, A. L., and Yang, L. Cocrxr: Contrastive captioners learn strong temporal structures for chest x-ray vision-language understanding. In *International Conference on Medical Image Computing and Computer-Assisted Intervention*, pp. 78–88. Springer, 2025.
- Cho, Y., Kim, T., Shin, H., Cho, S., and Shin, D. Pretraining vision-language model for difference visual question answering in longitudinal chest x-rays. *arXiv preprint arXiv:2402.08966*, 2024.
- Devlin, J., Chang, M.-W., Lee, K., and Toutanova, K. Bert: Pre-training of deep bidirectional transformers for language understanding. In *Proceedings of the 2019 conference of the North American chapter of the association for computational linguistics: human language technologies, volume 1 (long and short papers)*, pp. 4171–4186, 2019.
- Fini, E., Shukor, M., Li, X., Dufter, P., Klein, M., Haldimann, D., Aitharaju, S., da Costa, V. G. T., Béthune, L., Gan, Z., et al. Multimodal autoregressive pre-training of large vision encoders. In *Proceedings of the Computer Vision and Pattern Recognition Conference*, pp. 9641–9654, 2025.
- Goldberger, A. L., Amaral, L. A. N., Glass, L., Hausdorff, J. M., Ivanov, P. C., Mark, R. G., Mietus, J. E., Moody, G. B., Peng, C.-K., and Stanley, H. E. Physiobank, physiotoolkit, and physionet: Components of a new research resource for complex physiologic signals. *Circulation*, 101(23):e215–e220, 2000. URL <https://www.ahajournals.org/doi/full/10.1161/01.CIR.101.23.e215>. RRID:SCR\_00734.
- He, K., Chen, X., Xie, S., Li, Y., Dollár, P., and Girshick, R. Masked autoencoders are scalable vision learners. In *Proceedings of the IEEE/CVF conference on computer vision and pattern recognition*, pp. 16000–16009, 2022a.
- He, S., Guo, T., Dai, T., Qiao, R., Wu, C., Shu, X., and Ren, B. Vlmac: Vision-language masked autoencoder. *arXiv preprint arXiv:2208.09374*, 2022b.
- Hu, X., Gu, L., An, Q., Zhang, M., Liu, L., Kobayashi, K., Harada, T., Summers, R. M., and Zhu, Y. Expert knowledge-aware image difference graph representation learning for difference-aware medical visual question answering. In *Proceedings of the 29th ACM SIGKDD Conference on Knowledge Discovery and Data Mining, KDD ’23*, pp. 4156–4165. ACM, August 2023a. doi: 10.1145/3580305.3599819. URL <http://dx.doi.org/10.1145/3580305.3599819>.
- Hu, X., Gu, L., An, Q., Zhang, M., Liu, L., Kobayashi, K., Harada, T., Summers, R. M., and Zhu, Y. Expert knowledge-aware image difference graph representation learning for difference-aware medical visual question answering. In *Proceedings of the 29th ACM SIGKDD Conference on Knowledge Discovery and Data Mining*, pp. 4156–4165, 2023b.
- Huang, S.-C., Shen, L., Lungren, M. P., and Yeung, S. Gloria: A multimodal global-local representation learning framework for label-efficient medical image recognition. In *Proceedings of the IEEE/CVF international conference on computer vision*, pp. 3942–3951, 2021.
- Jia, C., Yang, Y., Xia, Y., Chen, Y.-T., Parekh, Z., Pham, H., Le, Q., Sung, Y.-H., Li, Z., and Duerig, T. Scaling up visual and vision-language representation learning with noisy text supervision. In *International conference on machine learning*, pp. 4904–4916. PMLR, 2021.
- Johnson, A., Lungren, M., Peng, Y., Lu, Z., Mark, R., Berkowitz, S., and Horng, S. MIMIC-CXR-JPG - chest radiographs with structured labels (version 2.1.0), 2024a. URL <https://doi.org/10.13026/jsn5-t979>. RRID:SCR\_007345.

- Johnson, A., Pollard, T., Mark, R., Berkowitz, S., and Horng, S. MIMIC-CXR Database (version 2.1.0), 2024b. URL <https://doi.org/10.13026/4jqj-jw95>. RRID:SCR\_007345.
- Johnson, A. E. W., Pollard, T. J., Berkowitz, S. J., Greenbaum, N. R., Lungren, M. P., Deng, C.-y., Mark, R. G., and Horng, S. MIMIC-CXR, a de-identified publicly available database of chest radiographs with free-text reports. *Scientific Data*, 6(317), 2019. doi: 10.1038/s41597-019-0322-0. URL <https://doi.org/10.1038/s41597-019-0322-0>.
- Kwon, G., Cai, Z., Ravichandran, A., Bas, E., Bhotika, R., and Soatto, S. Masked vision and language modeling for multi-modal representation learning. *arXiv preprint arXiv:2208.02131*, 2022.
- Li, C., Wong, C., Zhang, S., Usuyama, N., Liu, H., Yang, J., Naumann, T., Poon, H., and Gao, J. Llava-med: Training a large language-and-vision assistant for biomedicine in one day, 2023a. URL <https://arxiv.org/abs/2306.00890>.
- Li, J., Li, D., Savarese, S., and Hoi, S. Blip-2: Bootstrapping language-image pre-training with frozen image encoders and large language models. In *International conference on machine learning*, pp. 19730–19742. PMLR, 2023b.
- Li, L. H., Zhang, P., Zhang, H., Yang, J., Li, C., Zhong, Y., Wang, L., Yuan, L., Zhang, L., Hwang, J.-N., et al. Grounded language-image pre-training. In *Proceedings of the IEEE/CVF conference on computer vision and pattern recognition*, pp. 10965–10975, 2022.
- Lin, C.-Y. Rouge: A package for automatic evaluation of summaries. In *Text summarization branches out*, pp. 74–81, 2004.
- Liu, J., Zhou, H.-Y., Li, C., Huang, W., Yang, H., Liang, Y., Shi, G., Zheng, H., and Wang, S. Mlip: medical language-image pre-training with masked local representation learning. In *2024 IEEE International Symposium on Biomedical Imaging (ISBI)*, pp. 1–5. IEEE, 2024.
- Lu, Z., Xie, Y., Zeng, Q., Lu, M., Wu, Q., and Xia, Y. Spot the difference: Difference visual question answering with residual alignment. In Linguraru, M. G., Dou, Q., Feragen, A., Giannarou, S., Glocker, B., Lekadir, K., and Schnabel, J. A. (eds.), *Medical Image Computing and Computer Assisted Intervention – MICCAI 2024*, pp. 649–658, Cham, 2024. Springer Nature Switzerland. ISBN 978-3-031-72086-4.
- Papineni, K., Roukos, S., Ward, T., and Zhu, W.-J. Bleu: a method for automatic evaluation of machine translation. In *Proceedings of the 40th annual meeting of the Association for Computational Linguistics*, pp. 311–318, 2002.
- Radford, A., Wu, J., Child, R., Luan, D., Amodei, D., Sutskever, I., et al. Language models are unsupervised multitask learners. *OpenAI blog*, 1(8):9, 2019.
- Radford, A., Kim, J. W., Hallacy, C., Ramesh, A., Goh, G., Agarwal, S., Sastry, G., Askell, A., Mishkin, P., Clark, J., et al. Learning transferable visual models from natural language supervision. In *International conference on machine learning*, pp. 8748–8763. PmLR, 2021.
- Sellergren, A., Kazemzadeh, S., Jaroensri, T., Kiraly, A., Traverse, M., Kohlberger, T., Xu, S., Jamil, F., Hughes, C., Lau, C., Chen, J., Mahvar, F., Yatziv, L., Chen, T., Sterling, B., Baby, S. A., Baby, S. M., Lai, J., Schmidgall, S., Yang, L., Chen, K., Bjornsson, P., Reddy, S., Brush, R., Philbrick, K., Asiedu, M., Mezerreg, I., Hu, H., Yang, H., Tiwari, R., Jansen, S., Singh, P., Liu, Y., Azizi, S., Kamath, A., Ferret, J., Pathak, S., Vieillard, N., Merhej, R., Perrin, S., Matejovicova, T., Ramé, A., Riviere, M., Rouillard, L., Mesnard, T., Cideron, G., bastien Grill, J., Ramos, S., Yvinec, E., Casbon, M., Buchatskaya, E., Alayrac, J.-B., Lepikhin, D., Feinberg, V., Borgeaud, S., Andreev, A., Hardin, C., Dadashi, R., Hussenot, L., Joulin, A., Bachem, O., Matias, Y., Chou, K., Hassidim, A., Goel, K., Farabet, C., Barral, J., Warkentin, T., Shlens, J., Fleet, D., Cotruta, V., Sanseviero, O., Martins, G., Kirk, P., Rao, A., Shetty, S., Steiner, D. F., Kirmizibayrak, C., Pilgrim, R., Golden, D., and Yang, L. Medgemma technical report, 2025. URL <https://arxiv.org/abs/2507.05201>.
- Serra, F. D., Schrempf, P., Wang, C., Meng, Z., Deligianni, F., and O’Neil, A. Q. Grounding chest x-ray visual question answering with generated radiology reports. *arXiv preprint arXiv:2505.16624*, 2025.
- Tong, S., Liu, Z., Zhai, Y., Ma, Y., LeCun, Y., and Xie, S. Eyes wide shut? exploring the visual shortcomings of multimodal llms. In *Proceedings of the IEEE/CVF Conference on Computer Vision and Pattern Recognition*, pp. 9568–9578, 2024.
- Tschannen, M., Kumar, M., Steiner, A., Zhai, X., Houlsby, N., and Beyer, L. Image captioners are scalable vision learners too. *Advances in Neural Information Processing Systems*, 36:46830–46855, 2023.
- Vaswani, A., Shazeer, N., Parmar, N., Uszkoreit, J., Jones, L., Gomez, A. N., Kaiser, Ł., and Polosukhin, I. Attention is all you need. *Advances in neural information processing systems*, 30, 2017.
- Vedantam, R., Lawrence Zitnick, C., and Parikh, D. Cider: Consensus-based image description evaluation. In *Pro-*

- ceedings of the IEEE conference on computer vision and pattern recognition*, pp. 4566–4575, 2015.
- Wan, B., Tschannen, M., Xian, Y., Pavetic, F., Alabdulmohsin, I. M., Wang, X., Susano Pinto, A., Steiner, A., Beyer, L., and Zhai, X. Locca: Visual pretraining with location-aware captioners. *Advances in Neural Information Processing Systems*, 37:116355–116387, 2024.
- Wu, J., Agu, N., Lourentzou, I., Sharma, A., Paguio, J., Yao, J. S., Dee, E. C., Mitchell, W., Kashyap, S., Giovannini, A., Celi, L. A., Syeda-Mahmood, T., and Moradi, M. Chest ImaGenome Dataset (version 1.0.0), 2021. URL <https://doi.org/10.13026/wv01-y230>. RRID:SCR\_007345.
- Yang, X., Miao, J., Yuan, Y., Wang, J., Dou, Q., Li, J., and Heng, P.-A. Medical large vision language models with multi-image visual ability. In *International Conference on Medical Image Computing and Computer-Assisted Intervention*, pp. 402–412. Springer, 2025.
- Yao, L., Wang, W., and Jin, Q. Image difference captioning with pre-training and contrastive learning. In *Proceedings of the AAAI Conference on Artificial Intelligence*, volume 36, pp. 3108–3116, 2022.
- Zhai, X., Mustafa, B., Kolesnikov, A., and Beyer, L. Sigmoid loss for language image pre-training. In *Proceedings of the IEEE/CVF international conference on computer vision*, pp. 11975–11986, 2023.
- Zhang, H., Zhang, P., Hu, X., Chen, Y.-C., Li, L. H., Dai, X., Wang, L., Yuan, L., Hwang, J.-N., and Gao, J. Glipv2: unifying localization and vl understanding. In *36th Conf. Neural Inf. Process. Syst. NeurIPS*, 2022.
- Zhang, S., Xu, Y., Usuyama, N., Xu, H., Bagga, J., Tinn, R., Preston, S., Rao, R., Wei, M., Valluri, N., Wong, C., Tupini, A., Wang, Y., Mazzola, M., Shukla, S., Liden, L., Gao, J., Crabtree, A., Piening, B., Bifulco, C., Lungren, M. P., Naumann, T., Wang, S., and Poon, H. Biomedclip: a multimodal biomedical foundation model pretrained from fifteen million scientific image-text pairs, 2025. URL <https://arxiv.org/abs/2303.00915>.
- Zhang, T., Kishore, V., Wu, F., Weinberger, K. Q., and Artzi, Y. Bertscore: Evaluating text generation with bert. *arXiv preprint arXiv:1904.09675*, 2019.
- Zhang, X., Wu, C., Zhao, Z., Lin, W., Zhang, Y., Wang, Y., and Xie, W. Pmc-vqa: Visual instruction tuning for medical visual question answering, 2024. URL <https://arxiv.org/abs/2305.10415>.